ANNALS of Clinical and Translational Neurology
Open Access
ANA American Neurological Association since 1875

RESEARCH ARTICLE

SOD1 silencing in motoneurons or glia rescues neuromuscular function in ALS mice

Elisabeth Dirren[a], Julianne Aebischer [a], Cylia Rochat, Christopher Towne, Bernard L. Schneider & Patrick Aebischer

Brain Mind Institute, Ecole Polytechnique Fédérale de Lausanne EPFL, Lausanne, Switzerland

Correspondence
Bernard L. Schneider or Patrick Aebischer, EPFL SV BMI LEN, Station 19, 1015 Lausanne, Switzerland. Tel: +41 21 693 95 05; Fax: +41 21 693 95 20; E-mails: patrick.aebischer@epfl.ch, bernard.schneider@epfl.ch

Funding Information
E. D. was supported by a fellowship of the Swiss Foundation for Research on Muscle Diseases (FSRMM). The experimental work was supported by a grant of the Thierry Latran Foundation and by the SwissTransMed Platforms for Translational Research in Medicine.

Received: 20 November 2014; Accepted: 24 November 2014

***Annals of Clinical and Translational Neurology* 2015; 2(2): 167–184**

doi: 10.1002/acn3.162

[a]Both authors equally contributed to this study.

Abstract

Objective: Amyotrophic lateral sclerosis is an incurable disorder mainly characterized by motoneuron degeneration. Mutations in the superoxide dismutase 1 (SOD1) gene account for 20% of familial forms of the disease. Mutant SOD1 exerts multiple pathogenic effects through the gain of toxic properties in both neurons and glial cells. Here, we compare AAV-based gene therapy suppressing expression of mutant SOD1 in either motoneurons or astrocytes. **Methods**: AAV vectors encoding microRNA against human SOD1 were administered to ^{G93A}SOD1 mice either by intracerebroventricular injections in pups or by lumbar intrathecal injections in adults. Vector systems were designed to suppress SOD1 expression predominantly in either spinal motoneurons or astrocytes. Electrophysiological and behavioral tests were performed on treated animals to evaluate disease progression. **Results**: Following vector injection in ^{G93A}SOD1 pups, efficient silencing of SOD1 expression was achieved in motoneurons and/or astrocytes. Most complete protection of motor units was obtained when targeting human SOD1 predominantly in motoneurons. Suppressing SOD1 mainly in astrocytes led to preserved muscle innervation despite only partial protection of spinal motoneurons. In both cases, injection in pups led to full recovery of neuromuscular function and significantly prolonged survival. Vector injections in adult mice also achieved significant protection of neuromuscular function, which was highest when motoneurons were targeted. **Interpretation**: These results suggest that AAV-mediated SOD1 silencing is an effective approach to prevent motoneuron degeneration caused by SOD1 mutation. AAV vectors suppressing SOD1 in motoneurons delay disease onset and show effective neuroprotection. On the other hand, AAV-based SOD1 silencing in astrocytes rescues neuromuscular function following initial denervation.

Introduction

Amyotrophic lateral sclerosis (ALS) is a fatal neurodegenerative disorder that is characterized by the loss of cortical and spinal motoneurons, which results in progressive paralysis of most skeletal muscles. There is currently no cure for ALS and the disease ultimately leads to death within an average of 3–5 years after diagnosis has been made. While the precise etiology of ALS remains unclear, 10% of patients present an inherited form of the disease. Among them, 20% have a mutation in the gene encoding superoxide dismutase 1 (SOD1).[1] To date, over 160 mutations have been identified in SOD1, typically leading to a gain of toxic activity ultimately causing the degeneration of motoneurons, regardless of alterations in enzymatic activity.[2] Overall, mutant SOD1 can perturb a number of cellular functions, which collectively contribute to motoneuron degeneration.[3] In this setting, silencing mutant SOD1 expression appears as a logical therapeutic approach to counteract its toxicity.

Over the past several years, a few research groups including our laboratory have intensively aimed at targeting SOD1 mRNA by RNA interference (RNAi). Transgenic animals that overexpress human mutant SOD1 (SOD1 mice) develop a motor phenotype that closely mimics human disease and therefore constitute an effective

model to assess the therapeutic potential of SOD1 silencing strategies.[4] To achieve long-term expression of the silencing instructions in cells relevant for pathogenesis, lots of efforts have been put into developing viral gene delivery systems to target the central nervous system (CNS) and efficiently knockdown human SOD1. [5,6]

Recently, a major therapeutic breakthrough has been achieved using a single intravenous injection of serotype 9 adeno-associated viral (AAV) vector encoding shRNA against human SOD1.[7] When administrated at birth, AAV9 infects ~60% of motoneurons and 30% of astrocytes, which in the case of shRNA SOD1 expression translates into delayed disease onset, improved motor performances and around 40% extension in survival of treated mice. When injected into adult mice, AAV9 transduces more efficiently astrocytes (around 50%) than motoneurons (8%). Interestingly AAV9-shRNA remains therapeutic when delivered after disease onset and prolongs the survival of SOD1 mice, albeit to a lesser extent.

Based on these observations it remains to be determined what is the respective therapeutic contribution of AAV-based targeting of mutated SOD1 either in motoneurons or in astrocytes, a critical question to design the most effective approach for silencing SOD1. Indeed, in vitro experiments as well as investigations performed in SOD1 mice have revealed noncell autonomous disease processes.[8] While the expression of mutant SOD1 in motoneurons is required for disease onset, SOD1 pathology in non-neuronal cell types plays a key role in disease progression. In particular, removal of mutant SOD1 in astrocytes, or spinal cord enrichment in wild-type (WT) astrocytes ameliorates disease outcome of SOD1 animals.[9–12]

We use a combination of AAV vectors and promoters to deliver silencing cues to the spinal cord, while simultaneously providing some specificity regarding the targeted cells. Indeed, we have recently reported that intracerebroventricular (ICV) delivery of AAV6 combined with a cmv promoter allows targeting up to 80% of spinal motoneurons in newborn mice, while ICV injection of AAV9 combined to the gfaABC$_1$D promoter achieves transgene expression in at least 50% of ventral horn astrocytes.[13] Here, we use AAV vectors to silence SOD1 through overexpression of artificial microRNAs (miRNA) under the control of polymerase II promoters, to compare the therapeutic efficacy of motoneuronal versus astrocytic SOD1 silencing. We show that overexpression of miRNAs against SOD1 (miR SOD1) in motoneurons and/or astrocytes, rescues electrophysiological, and motor abnormalities in ^{G93A}SOD1 mice. Highest therapeutic benefit using AAV vectors is observed when SOD1 silencing clues are directed toward motoneurons.

Materials and Methods

Preparation of AAV vectors

Shuttle plasmids for AAV6 production were produced by cloning the cmv:RFP cassette into a pAAV-MCS plasmid (Stratagene, La Jolla, CA). Plasmids for AAV9 production were designed by cloning GFP under the minimal GFAP promoter gfaABC$_1$D (kindly provided by Dr M. Brenner, Department of Neurobiology, University of Alabama) into the pAAV-MCS plasmid. Following microRNA sequences were used to target human SOD1: miR SOD1: 5′-ATT ACT TTC CTT CTG CTC GAA-3′, 5′-miR-b SOD1: AAT CCA TGC AGG CCT TCA GTC-3′, miR cont: 5′-AAA TGT ACT GCG CGT GGA GAC-3′. Invitrogen Block-iT RNAi Designer (Invitrogen, Molecular Probes, Carlsbad, CA) was used to design these 21 nucleotide sequences targeting human SOD1 coding sequence, and no other known sequence in the mouse genome. These miR sequences were then introduced into the pre-miRNA backbone of murine miR-155. The corresponding DNA sequence was synthesized by Dundee Cell Products (Dundee Cell Products, Dundee, Scotland, UK) and subcloned in series with GFP or RFP in the pAAV shuttle plasmid according to standard procedures. Shuttle plasmids were cotransfected with pDP6 or pDF9 helper plasmids into HEK293-AAV cells (Agilent Technologies, Santa Clara, CA) for production of recombinant AAV6 and AAV9, respectively. Cells were lysed 48 h following transfection and viral particles were sequentially purified on iodixanol and heparin affinity columns. Viral genomic copies were measured by TaqMan qPCR (Invitrogen) using primers recognizing the human β-globin intron.

Transfection of HEK293T cells

pAAV were delivered into HEK293T cells by calcium phosphate transfection. Proteins were extracted in a 1% NP40 lysis buffer 48 h post-transfection. Protein concentration was determined using a BCA protein assay kit (Thermo Fisher Scientific, Rockford, IL). About 30 μg of protein per condition were loaded and separated on a 12% acrylamide gel. Following transfer to a nitrocellulose membrane, human SOD1 was revealed by overnight incubation in an anti-human SOD1 antibody (clone SD-G6; Sigma-Aldrich, St-Louis, MO) followed by two hrs incubation in a secondary Alexa Fluor 680 rabbit anti-mouse antibody (Invitrogen). Actin was used as loading control and revealed with a goat anti-actin primary antibody (Santa Cruz Biotechnology, Dallas, TX) and rabbit anti-goat Alexa Fluor 680 secondary antibody (Invitrogen). Protein bands were detected using an Odyssey scanner

(LI-COR Biosciences, Lincoln, NE) and quantified with the ImageJ software.

Administration of viral vectors

All animal works were performed in accordance with the Swiss legislation and the European Community Council directive (86/609/EEC) for the care and use of laboratory animals. For this proof-of-principle study, B6.Cg-Tg (SOD1*G93A)^{dl}1Gur/J mice (The Jackson Laboratory, Bar Harbor, ME) were mated with C57BL/6J females (Charles River Laboratories, Bois des Oncins, France) to obtain mice on a pure background, promoting phenotypic uniformity, which allows to assess disease progression in cohorts smaller than what is recommended for the non-congenic background.[14] Newborn pups were genotyped at birth by PCR against human SOD1. Intramuscular injections were performed on postnatal day 2 (P2). Two microliter of virus were delivered into the gastrocnemius muscle using a 30G insulin needle attached to a 10 μL Hamilton syringe (Hamilton, Reno, NV) by a polyethylene catheter. Mice were transcardially perfused with phosphate buffered saline (PBS) 3 weeks following injection. Gastrocnemius muscles were recovered, frozen on dry ice and stored at −80°C. For ICV injections, P2 pups were anesthetized with a combination of medetomidine (Dorbene®; Dr. Graeub AG, Bern, Switzerland) and midazolam (Dormicum®; Roche, Basel, Switzerland). Virus was diluted in a physiologic sodium chlorine solution and mixed with 0.1% Fast Green FCF (Sigma-Aldrich) to visualize spread of the virus into the ventricles. Three microliters of viral preparation were injected into the left lateral ventricle using a 29G insulin syringe. Reversal of anesthesia was performed by subcutaneous injection of atipamezole (Alzane®; Dr. Graeub AG, Bern, Switzerland). For IT injections, 5-week-old mice were anesthetized using isoflurane. Ten microliters of viral suspension was injected into the mouse lumbar subarachnoid space using a 30G insulin syringe. In brief, the insulin needle was inserted perpendicularly to the spinal cord at the level of the pelvic bones. When the syringe touched a vertebra it was tilted horizontally to an angle of ~60° with needle pointing in direction of the head. When finding a space between two vertebras, the needle was further inserted to reach the subarachnoid space. Viral suspension was injected when tail flick was observed.

Electrophysiology, swimming test, rotarod, and further animal handling

Compound muscular action potentials (CMAP) were measured on isoflurane-anesthetized mice using electromyographic apparatus (Keypoint, Dantec, Les Ulis, France or AD Instruments, Oxford, UK). Briefly, the sciatic nerve was stimulated nonspecifically by two electrodes placed over the lumbar vertebral column. CMAP was recorded by two electrodes placed in the belly and in the tendon of the right gastrocnemius muscle. A reference earth electrode was placed in the left gastrocnemius and connected to electromyography apparatus.

The swimming tank test was performed in a narrow Plexiglas pool with a visible escape platform placed at one extremity. Time to reach the 1 m distant platform was measured. For the Rotarod test the rotating wheel was set to accelerate from 4 to 40 rpm in 300 sec and for each mouse the latency to fall was recorded in seconds. Transgenic animals displaying typical hindlimb paralysis were sacrificed when not able to right themselves over a 20 sec period of time. AAV-injected mice that instead presented other signs and symptoms of systemic dysfunctions were sacrificed when resulting discomfort justified it. Quadriceps muscles were recovered, frozen on dry ice, and kept at −80°C. One gastrocnemius muscle was embedded in Cryomatrix (Thermo Fisher Scientific), frozen on dry ice and kept at −20°C for fiber area analysis. Animals were further perfused with paraformaldehyde (PFA) 4%. The second gastrocnemius muscle and spinal cord were postfixed in PFA 4% and transferred in a 35% sucrose solution prior to further handling.

Quantification of human SOD1 level in muscles

Fresh frozen gastrocnemius or quadriceps muscles were defrosted and sonicated in T-Per protein extraction buffer (Thermo Fisher Scientific). About 30 μg of protein were loaded on a 12% acrylamide gel. After migration and transfer to a nitrocellulose membrane, human SOD1 and actin were detected and quantified as described above.

Histological analysis

About 25 μm spinal cord sections were cut on a cryostat and conserved free floating in azide-PBS solution. Around 25 or 20 μm gastrocnemius sections were directly mounted on glass slides. For immunostaining, sections were incubated in a 0.15% Triton X-100, 5% bovine serum albumin (BSA), 3% serum blocking solution for 2 h at room temperature (RT). Sections were then incubated overnight at 4°C with the primary antibody diluted in blocking solution. Sections were sequentially washed and incubated with the secondary antibody diluted in blocking solution for 2 h at room temperature. After another washing step, sections were mounted with Mowiol (Sigma-Aldrich). Following primary antibodies were used: mouse anti-human SOD1 (clone SD-G6,

Sigma-Aldrich), rabbit anti-GFP (Invitrogen), mouse anti-GFP (Invitrogen), rabbit anti-RFP (Abcam, Cambridge, UK), goat anti-ChAT (Chemicon Millipore, Billerica, MA), rabbit anti-VAChT (Sigma-Aldrich), rabbit anti-GFAP (DakoCytomation, Glostrup, Denmark), rabbit anti-Iba1 (Wako Pure Chemical Industries, Osaka, Japan), rabbit anti-Olig2 (Chemicon Millipore). Secondary antibodies used included: donkey anti-mouse Alexa Fluor 488 (Invitrogen), goat anti-rabbit Alexa Fluor 488 (Invitrogen), goat anti-rabbit Cy3 (Jackson ImmunoResearch Laboratories, West Grove, PA), donkey anti-goat Alexa Fluor 647 (Invitrogen), goat anti-rabbit Alexa Fluor 647 (Invitrogen). For detection of GFP following IT injection, donkey anti-rabbit IgG Biotinylated (Jackson ImmunoResearch Laboratories) was used in combination with Streptavidin Alexa Fluor 488 (Invitrogen). For quantification of cell-type specificity following ICV injection of AAV6-cmv:GFP ($n = 4$ mice) or AAV9-gfaABC$_1$D:GFP vectors ($n = 4$), three lumbar sections per mouse were immunolabeled for GFP in combination with NeuN, VAChT, GFAP, IbaI, or Olig2. Pictures of the entire spinal cord sections were taken with a 10× objective on a Leica DM5500 microscope (Leica, Wetzlar, Germany). For animals injected with AAV6-cmv:GFP all GFP-expressing cells per section were evaluated for their colabeling with either one of the above mentioned markers. For those animals injected with AAV9-gfaABC$_1$D:GFP, 100 GFP-positive cells per section were randomly analyzed for colabeling. For evaluation of miR SOD1 silencing ability, spinal cord sections were stained against human SOD1 and ChAT for the AAV6:miR SOD1 condition or human SOD1 and GFAP for the AAV9:miR SOD1 condition ($n = 3$ per group). For each animal, confocal images from 20 RFP-expressing motoneurons (as identified by ChAT immunostaining) were produced with an inverted LSM 700 (Carl Zeiss, Oberkochen, Germany). Motoneurons were manually delimited and mean grey intensity was measured on the human SOD1 channel with the ImageJ software (National Institutes of Health, USA). Similarly, confocal images from 20 GFP-expressing astrocytes (identified by GFAP staining) were used for measurement of miR SOD1 silencing in astrocytes. For motoneuron counts, serial 25 μm sections separated by 500 μm were stained against ChAT. ChAT-positive motoneurons were then manually counted in the ventral horn of each spinal cord section using an Olympus AX70 microscope (Olympus Corporation, Shinjuku, Japan). Microglial activation was evaluated by manual counting of Iba1-positive microglia cells in the ventral horn of 10 lumbar spinal cord sections ($n = 5$ animals per group). Astroglial activation was assessed in the ventral horn of GFAP stained lumbar sections and pictured using a DM5500 microscope (Leica) (10 ventral horns per mouse, five mice per group). GFAP-positive total area was determined with ImageJ using percentile thresholding.

Neuromuscular junction (NMJ) occupancy was evaluated on 20 μm muscle sections stained with an anti-SV-2 (Developmental Studies Hybridoma Bank, University of Iowa, Iowa City, IA) or VAChT antibody and tetramethylrhodamine α-bungarotoxin (Invitrogen). About 100 bungarotoxin-positive motor end plates were identified and checked for overlapping SV-2 or VAChT-positive motoneuron terminal using an Olympus AX70 microscope or Leica DM5500 microscope ($n = 3$ animals per group for ICV injections and control animals; $n = 6$ for the IT AAV9-cmv group; $n = 7$ for the IT AAV9-gfaABC$_1$D group). For muscle fiber area analysis, gastrocnemius muscle tissue was processed without PFA fixation to avoid shrinkage. 25 μm sections were cut with a cryostat, and stained with a standard hematoxylin–eosin staining protocol. Five 600 × 400 μm fields of views were pictured per muscle with an Olympus AX70 microscope (Olympus Corporation) ($n = 5$ animals per group). Fiber area was determined for all visualized fibers using the ImageJ software.

Statistical analyses

Data are presented as mean ± standard deviation unless stated in the figure legend. One-way or two-way ANOVA and Newman–Keuls post hoc tests were performed with the Statistica software. Nonparametric survival and weight analysis were performed using the Cox-Mantel tests. All results with $P < 0.05$ were considered significant.

Results

miRNAs against SOD1 efficiently silence SOD1 expression *in vitro* and *in vivo*

Two different miRNA sequences were used to specifically target the coding sequence of human SOD1: miR SOD1 (target sequence: nt. 209-229, NM_000454.4) and miR-b SOD1 (nt. 265-285) were selected for in vitro and in vivo assessments of silencing efficiency. A scramble miR sequence (miR cont) was designed as control. These sequences were cloned in series with RFP under a cmv promoter and packaged in AAV6 capsids, a system which was previously found effective for expression in spinal motoneurons[13] (Fig. 1A). AAV9 recombinant particles encoding GFP in series with miR sequences, both under the control of the gfaABC$_1$D promoter, were produced for astrocyte-specific expression (Fig. 1A).[13] Silencing efficacy was tested by cotransfecting pAAV-cmv:RFP:miR SOD1, pAAV-cmv:RFP:miR-b SOD1, or pAAV-cmv:RFP:miR cont constructs with a cmv:^{G93A}SOD1 construct in

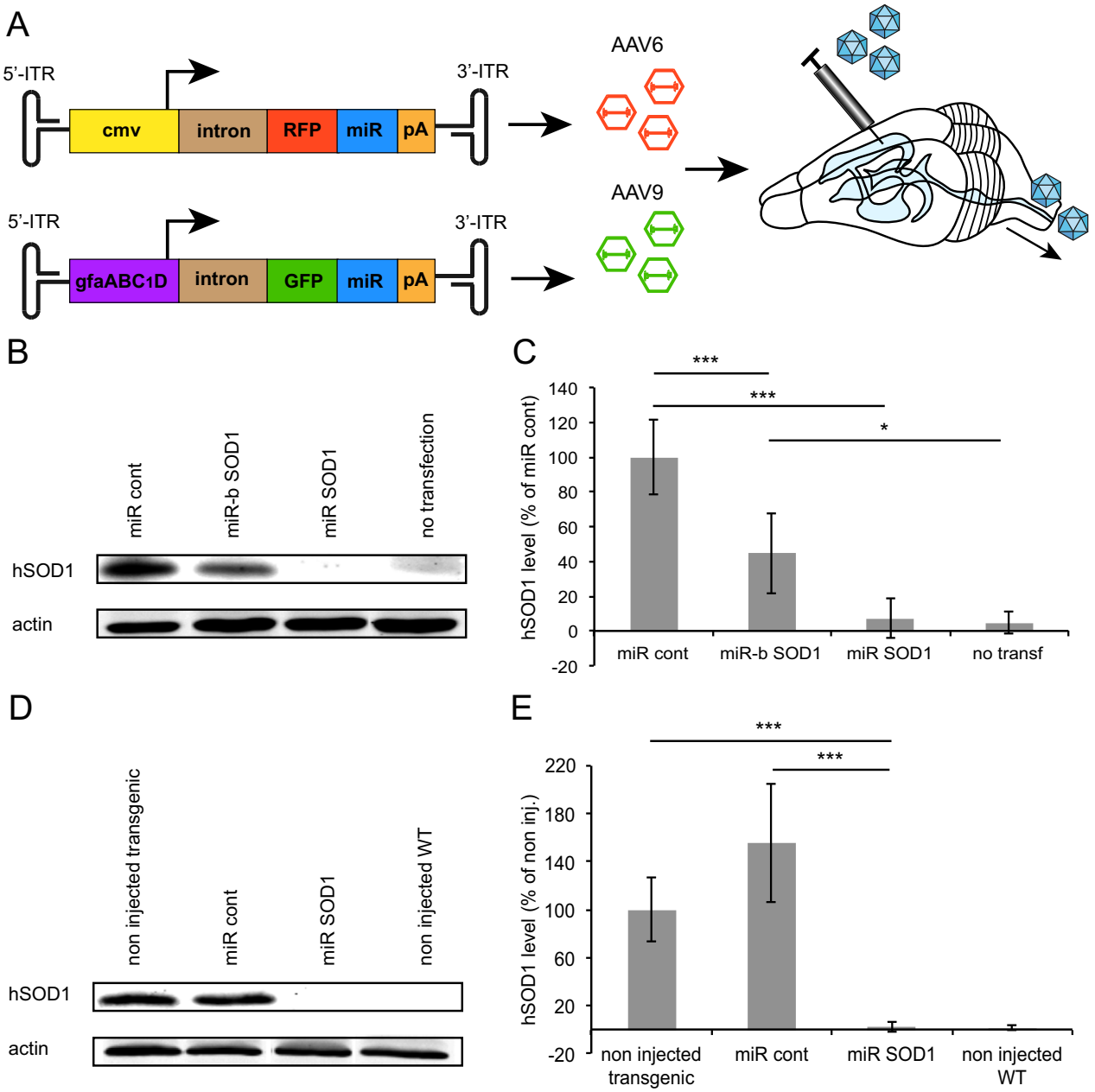

Figure 1. Silencing of SOD1 expression by overexpression of miRNA against human SOD1 coding sequence. (A) Experimental design for overexpression of miRNA SOD1 in motoneurons and/or astrocytes of ^{G93A}SOD1 mice. (B) Western blot depicting human SOD1 (hSOD1) levels following transient cotransfection of pAAV-cmv:RFP:miR SOD1, pAAV-cmv:RFP:miR-b SOD1 or pAAV-cmv:RFP:miR cont with a cmv:^{G93A}SOD1 construct in HEK293T cells. (C) Quantification of human SOD1 levels relative to miR cont condition following overexpression of miR SOD1, miR-b SOD1 or miR control in HEK293T cells. Human SOD1 expression is significantly reduced in cells overexpressing miR SOD1 and to a lesser extent miR-b SOD1. (D) Western blot of triceps surae total protein extracts of ^{G93A}SOD1 mice 3 weeks following intramuscular injection of AAV6-cmv:RFP:miR SOD1 or AAV6-cmv:RFP:miR cont; $n = 4$ per condition. (E) Quantification of human SOD1 level in the triceps surae of ^{G93A}SOD1 mice, 3 weeks post-intramuscular delivery of AAV6-cmv:RFP:miR SOD1 or AAV6-cmv:RFP:miR cont. Human SOD1 expression is almost completely suppressed in muscles of the AAV6:miR SOD1 group. Values are expressed as percentage of human SOD1 level in transgenic noninjected animals; $n = 4$ per condition. In vitro experiments were done in triplicates. $^*P < 0.05$, $^{***}P < 0.001$, one-way ANOVA and Newman–Keuls post hoc test. Data are expressed as mean ± standard deviations. SOD1, superoxide dismutase 1.

HEK293T cells. The miR SOD1 sequence was the most effective for SOD1 silencing, leading to near complete suppression of ^{G93A}SOD1 expression (Fig. 1B and C). When miR-b SOD1 was overexpressed, ^{G93A}SOD1 level was significantly reduced to 45 ± 23% of the miR cont condition. In order to assess in vivo the functionality of the most efficient miR SOD1 sequence, 8.4E9 viral genomic copies (vg) of AAV6-cmv:RFP:miR SOD1 were injected in the triceps surae of newborn ^{G93A}SOD1 mice. Western blot performed on muscle protein extracts

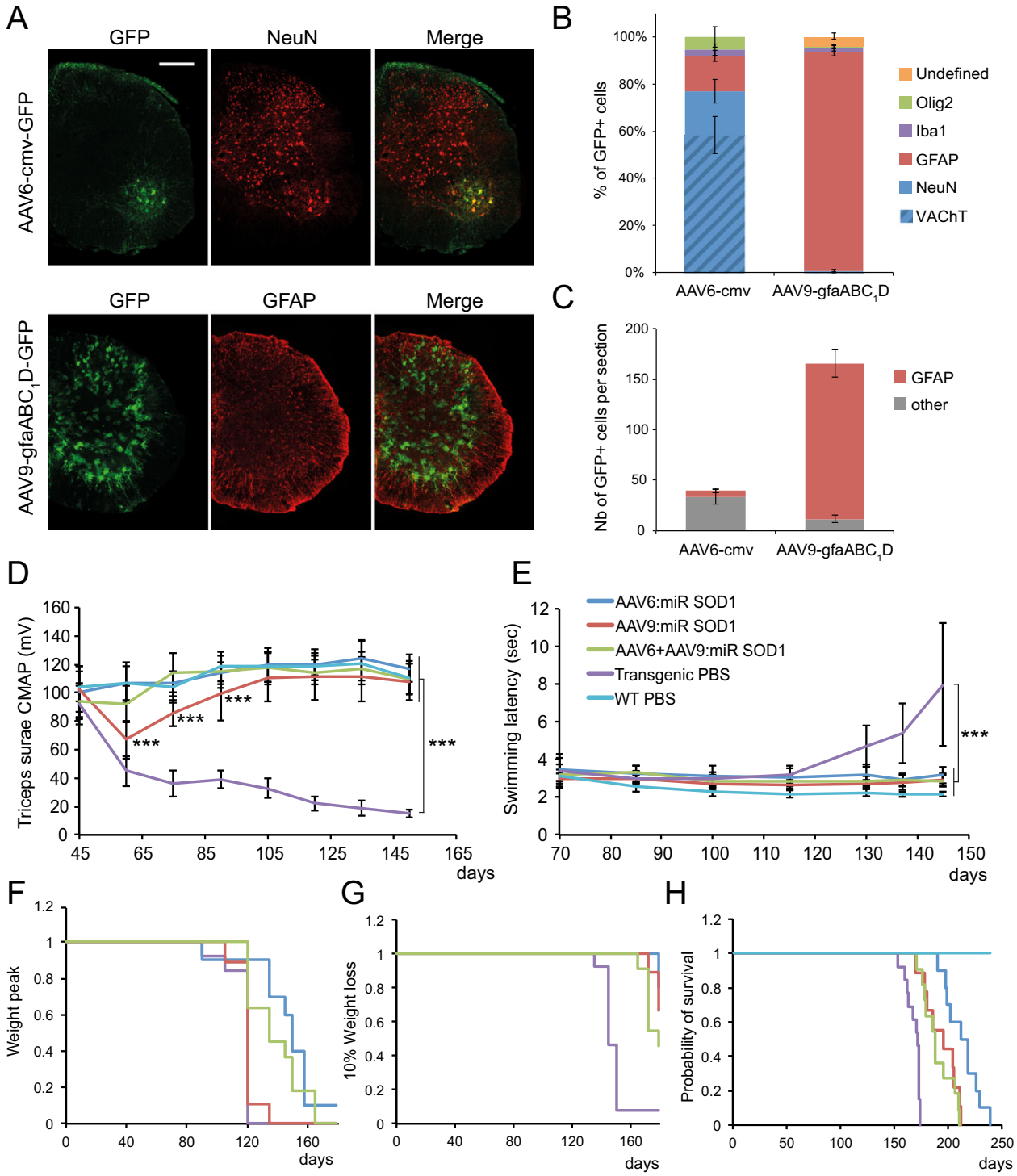

Figure 2. AAV-mediated silencing of human SOD1 in motoneurons and/or astrocytes rescues neuromuscular function and increases lifespan of ^{G93A}SOD1 mice. (A) Following ICV injection of newborn mice, AAV6 coupled with the cmv promoter preferentially leads to GFP expression in NeuN-positive motoneurons, whereas AAV9-gfaABC$_1$D specifically targets astrocytes. Represented are hemisections of lumbar spinal cords immunolabeled for GFP and either NeuN or GFAP. Scale bar: 250 μm. (B) Quantification of the percentage of GFP-positive cells colabeling with either NeuN, VAChT, GFAP, Iba1 or Olig-2 following ICV injection of AAV6-cmv:GFP or AAV9-gfaABC$_1$D:GFP. Animals per group: $n = 4$. (C) Representation of the absolute number of GFP-positive astrocytes found per spinal cord section following ICV injection of AAV6-cmv:GFP or AAV9-gfaABC$_1$D:GFP. (D) Compound muscular action potential (CMAP) values representing neuromuscular function were recorded from triceps surae of treated and control animals. Neuromuscular function appears to be maintained in AAV-injected animals compared to transgenic controls. AAV6:miR SOD1: $n = 10$, AAV9:miR SOD1: $n = 9$, AAV6 + AAV9:miR SOD1: $n = 11$, transgenic PBS: $n = 13$, WT PBS: $n = 15$. Note that CMAP values are significantly decreased at days 60, 75, and 90 in the AAV9:miR SOD1 group with respect to WT PBS ($P < 0.001$). (E) Swimming performance over disease course reveals improved motor abilities in treated animals. AAV6:miR SOD1: $n = 8$, AAV9:miR SOD1: $n = 9$, AAV6 + AAV9:miR SOD1: n = 10, transgenic PBS: $n = 13$, WT PBS: $n = 15$. (F) Kaplan–Meier representing disease onset, as defined by the day when mice reach their peak body weight. AAV6:miR SOD1 significantly delays median disease onset by 30 days when compared to PBS-injected ^{G93A}SOD1 mice (transgenic PBS: 120 $\pm$ 5.6, AAV6:miR SOD1: 150 $\pm$ 21.5, AAV9:miR SOD1: 120 $\pm$ 7.5, AAV6 + AAV9:miR SOD1: 135 $\pm$ 17.6). (G) Kaplan–Meier representing entry into end disease stage, as defined by the time when mice show 10% weight loss from their peak body weight. AAV9:miR SOD1 significantly prolongs early disease phase by 34 days when compared to control animals. (H) Kaplan–Meier survival curve of AAV-injected and control animals. AAV6:miR SOD1: $n = 10$, AAV9:miR SOD1: $n = 9$, AAV6 + AAV9:miR SOD1: $n = 11$, transgenic PBS: $n = 13$, WT PBS: $n = 15$. Values are expressed as mean $\pm$ standard deviation. One-way ANOVA and Newman–Keuls post hoc test. Two-way ANOVA and Newman–Keuls post hoc test was used for evaluation of the significance of group effect on CMAP values and swimming performance. ***$P < 0.001$. SOD1, superoxide dismutase 1; ICV, intracerebroventricular; WT, wild-type.

3 weeks postinjection confirmed that miR SOD1 led to near complete silencing of human SOD1 expression (2 $\pm$ 4% of noninjected ^{G93A}SOD1 mice) (Fig. 1D). Human SOD1 level remained unchanged in mice injected with AAV6-cmv:RFP:miR cont (155 $\pm$ 50% of noninjected ^{G93A}SOD1 mice) (Fig. 1E).

AAV delivery of miR SOD1 to motoneurons and/or astrocytes significantly improves disease outcome of ^{G93A}SOD1 mice

Since the objective of this study was to compare therapeutic benefits with respect to targeted cell types, we first determined the cell specificity of AAV6-cmv and AAV9-gfaABC$_1$D vectors. P2 pups were injected ICV with AAV6-cmv:GFP or AAV9-gfaABC$_1$D:GFP and sacrificed 4 weeks later. The percentage of GFP-positive cells coexpressing either neuronal markers (NeuN or VAChT) or non-neuronal markers (GFAP, Iba1 or Olig2) was quantified in the spinal cord. AAV6-cmv:GFP led to expression of GFP mainly in NeuN-positive neurons (81.4 $\pm$ 5.3%), among which about 75% were positive for VAChT. The majority of remaining GFP-positive cells expressed the astrocyte marker GFAP (15.7 $\pm$ 2.4%) (Fig. 2A and B). However, the absolute number of spinal astrocytes expressing GFP remained low, with an average of 6 $\pm$ 2 cells per spinal cord section, compared to 154 $\pm$ 13 for AAV9-gfaABC$_1$D:GFP injected animals (Fig. 2C). Indeed, nearly all GFP-positive cells were immunoreactive for GFAP (92.8 $\pm$ 1.6%) following ICV injection of AAV9-gfaABC$_1$D:GFP (Fig. 2A and B).

AAV vectors were then administered to the CNS of ^{G93A}SOD1 mice, in order to reduce human SOD1 levels predominantly in spinal motoneurons (AAV6-cmv) or astrocytes (AAV9-gfaABC$_1$D). Vectors were first ICV injected in mouse neonates to maximize transduction efficiency across the CNS and to assess neuroprotective potential of SOD1 silencing over the entire course of the disease. AAV vectors were produced according to optimized standard procedures and for this comparative study only batches with yields corresponding to highest achievable titer values were used for each serotype. Hence, P2 ^{G93A}SOD1 mice were injected with either 1.6E11 vg of AAV6-cmv:RFP:miR SOD1 or 6.8E11 vg of AAV9-gfaABC$_1$D:GFP:miR SOD1. As recently described, these vector doses allow targeting up to 80% of cervical and 70% of lumbar motoneurons for the AAV6-cmv vector and at least 50% of ventral horn astrocytes for the AAV9-gfaABC$_1$D vector.[13] A third group of animals was injected with a combination of both vectors. Because of volume restriction and to avoid potential vector overload, this group received each vector at only half of the dose used for single injections: 8E10 vg of AAV6-cmv:RFP:miR SOD1 and 3.4E11 vg of AAV9-gfaABC$_1$D:GFP:miR SOD1. Neuromuscular function was regularly assessed by measurement of the compound muscular action potential (CMAP) in triceps surae muscles. In PBS-injected ^{G93A}SOD1 mice, CMAP amplitude declined between postnatal days 50 and 60 (Fig. 2D). The amplitude then stabilized at around 40% of the starting value for 30 days before gradually decreasing until end stage. Remarkably, animals of the AAV6:miR SOD1 and AAV6 + AAV9:miR SOD1 groups displayed CMAP values comparable to WT controls over the whole study. Mice injected with AAV9-gfaABC$_1$D:GFP:miR SOD1 showed a significant decrease ($P < 0.001$ compared to PBS-injected WT mice) in CMAP values between days 50 and 60. However, this decrease was only transient and CMAP amplitude progressively

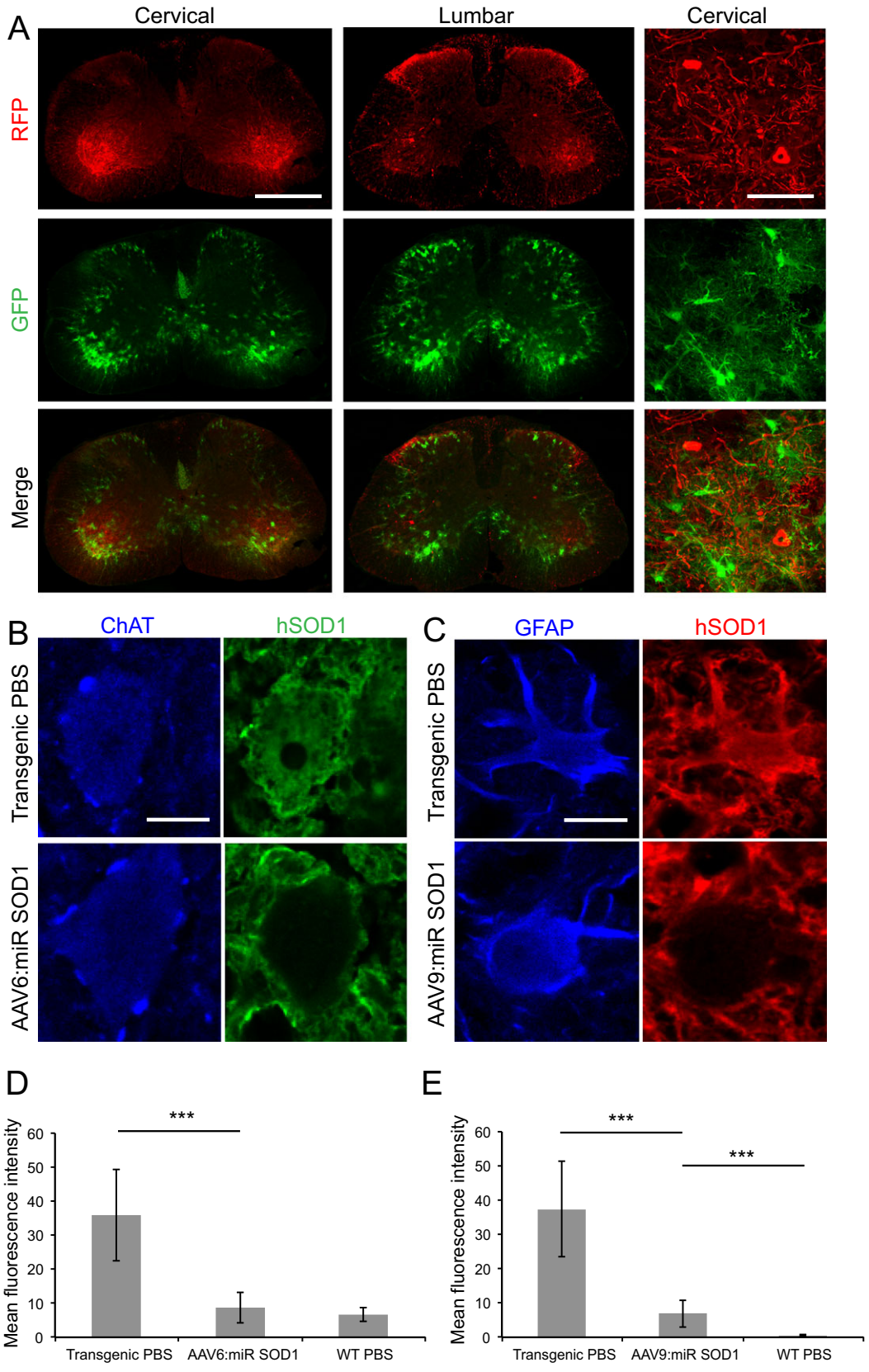

recovered until P100, time point at which it no longer statistically differed from PBS-injected WT mice.

Motor performance was assessed by measuring the time taken by the animals to swim to a distant platform. Control transgenic mice showed first signs of disability around day 120 (Fig. 2E). Swimming performance then rapidly deteriorated. Remarkably, none of the treated group experienced such worsening. Hence, both electrophysiological values and motor performance of mice overexpressing miR SOD1 in motoneurons and/or astrocytes remained close to normal values, suggesting preservation of neuromuscular function.

In ALS mice, weight variation is frequently used to determine disease onset (peak of the weight curve) and the phase of early disease progression (from onset to 10% weight loss).[15] In PBS-injected ^{G93A}SOD1 mice, weight peak was observed at a median of 120 ± 5.6 days (Fig. 2F). The median disease onset was significantly delayed by 30 and 15 days in the AAV6:miR SOD1 and AAV6 + AAV9:miR SOD1 groups, respectively. Of note, there was no significant difference between AAV9-gfaABC$_1$D:GFP:miR SOD1 and PBS-injected ^{G93A}SOD1 mice. However, AAV9-gfaABC$_1$D:GFP:miR SOD1 significantly prolonged the early disease phase when compared to control ^{G93A}SOD1 mice (Fig. 2G).

Overall, disease outcome was remarkably improved. The median survival of animals injected ICV with AAV6-cmv:RFP:miR SOD1 was 215 ± 16 days as compared to 171 ± 7 days for PBS-injected controls. A 44 days-increase in survival was hence achieved when silencing SOD1 in motoneurons (Fig. 2H). Though to a smaller extent, life expectancy was also increased in the AAV9:miR SOD1 (195 ± 16 days) and AAV6 + AAV9:miR SOD1 (188 ± 14 days) groups (Fig. 2H). Of note, none of the miR SOD1-treated animals had hindlimb paralysis at end stage, which was used as endpoint criteria for PBS-injected mice. Instead, miR SOD1-treated animals developed ataxia, increased susceptibility to skin and eye infection and gastrointestinal complications leading sometimes to sudden animal loss. Some of these symptoms justified euthanasia when the comfort of the animal was severely impaired. Overall, these results demonstrate that targeting either spinal motoneurons or astrocytes can significantly improve motor function and survival of ^{G93A}SOD1 mice, with motoneuronal SOD1 silencing leading to a better therapeutic outcome when compared to astrocytic SOD1 depletion.

To exclude the possibility that these effects were non-specific and merely due to overexpression of a miRNA, ^{G93A}SOD1 pups were injected with AAV6 and AAV9 vectors encoding either miR cont or miR-b SOD1 sequences. The exact same paradigm was applied for injections and follow-up of these mice as for miR SOD1-treated animals. Overexpression of miR cont had no effect on neuromuscular function and survival, while miR-b showed only modest, but significant improvement of swimming performance and survival (Fig. S1). Overall, the effects obtained were correlated with the SOD1 silencing efficacy of the overexpressed miR sequence, supporting the specificity of neuromuscular function rescue observed with miR SOD1.

Human SOD1 is repressed in motoneurons and/or astrocytes of miR SOD1-treated mice

We next sought to determine efficiency of human SOD1 repression in the spinal cord of treated mice at end stage. Expression of RFP and GFP was used to trace miR-expressing motoneurons and astrocytes, respectively, as these reporter proteins are synthesized from the precursor transcript of miR SOD1. As expected, RFP staining was found in ChAT-positive motoneurons of AAV6:miR SOD1 animals and GFP staining was observed in astrocytes of AAV9:miR SOD1 animals. Consistent with these observations, RFP and GFP segregated to motoneurons and astrocytes, respectively, in spinal cords of mice co-injected with AAV6-cmv:RFP:miR SOD1 and AAV9-gfaABC$_1$D:GFP:miR SOD1 (Fig. 3A). Confocal images of spinal cord sections costained for human SOD1 and

Figure 3. SOD1 expression is suppressed in motoneurons and astrocytes of end-stage animals injected with AAV-miR SOD1. (A) RFP and GFP expression in motoneurons or astrocytes, respectively, is conserved in end-stage animals injected with various vector combinations. Represented are cervical and lumbar sections of a mouse from the AAV6 + AAV9:miR SOD1 group. Scale bar: whole spinal cord, 500 μm; cervical close-up, 80 μm. (B) Human SOD1 expression in a motoneuron of a PBS-injected transgenic mouse as compared to an AAV6-cmv:RFP:miR SOD1 injected animal. Note the absence of human SOD1 labeling in the vector-injected condition. Scale bar: 15 μm. (C) Human SOD1 expression in astrocytes of a transgenic mouse injected with PBS or AAV9-gfaABC$_1$D:GFP:miR SOD1. In the latter group, note the loss of human SOD1 expression in the cell body of the GFAP-labeled astrocyte. Scale bar: 10 μm. (D) Immunolabeled human SOD1 level expressed as mean fluorescence intensity. Mean fluorescence intensity was randomly assessed in 20 motoneurons identified by ChAT immunostaining for each represented condition. Human SOD1 levels are significantly lower in end-stage animals injected with AAV6-cmv:RFP:miR SOD1 as compared to PBS-injected transgenic mice. (E) Mean fluorescence intensity following human SOD1 immunostaining in astrocytes of AAV9:miR SOD1, transgenic PBS or WT PBS groups. Note the silencing of human SOD1 expression in animals injected with AAV9-gfaABC$_1$D:GFP:miR SOD1. $N = 20$ motoneurons or astrocytes per animal, three animals per condition. ***$P < 0.001$, one-way ANOVA and Newman–Keuls post hoc test. Data are represented as mean ± standard deviation. SOD1, superoxide dismutase 1; WT, wild-type.

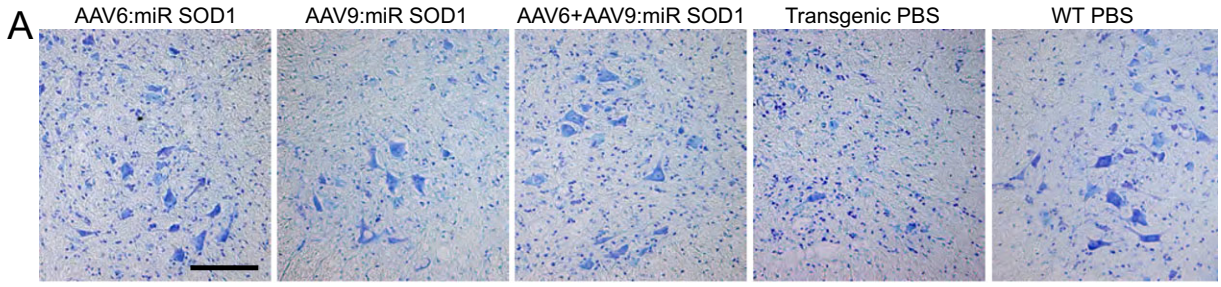

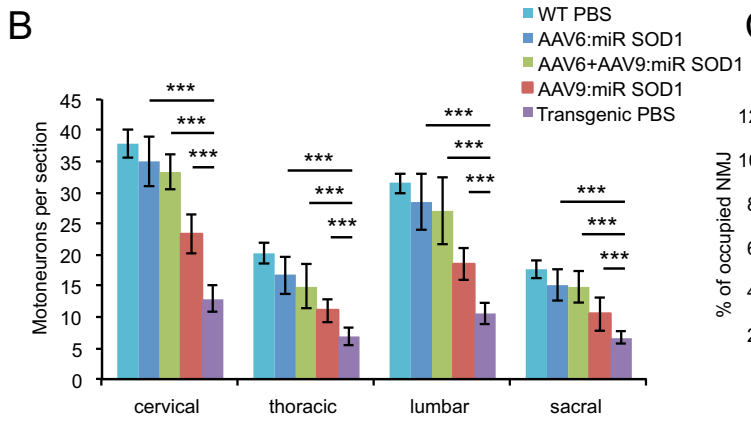

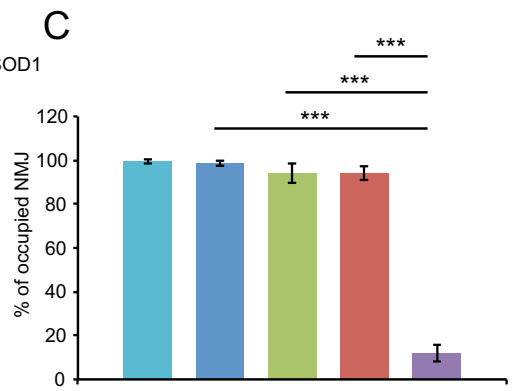

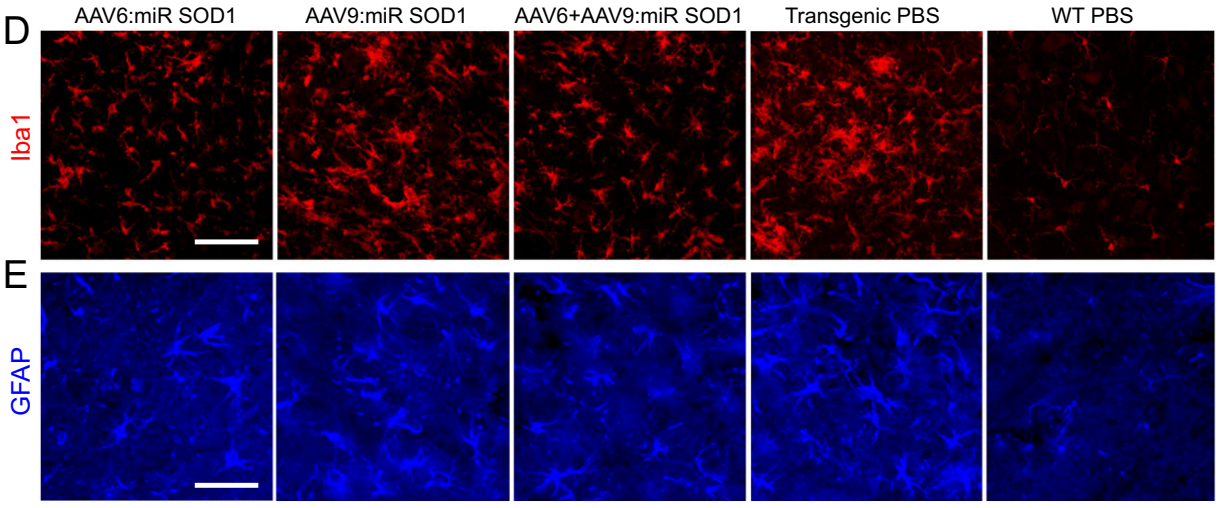

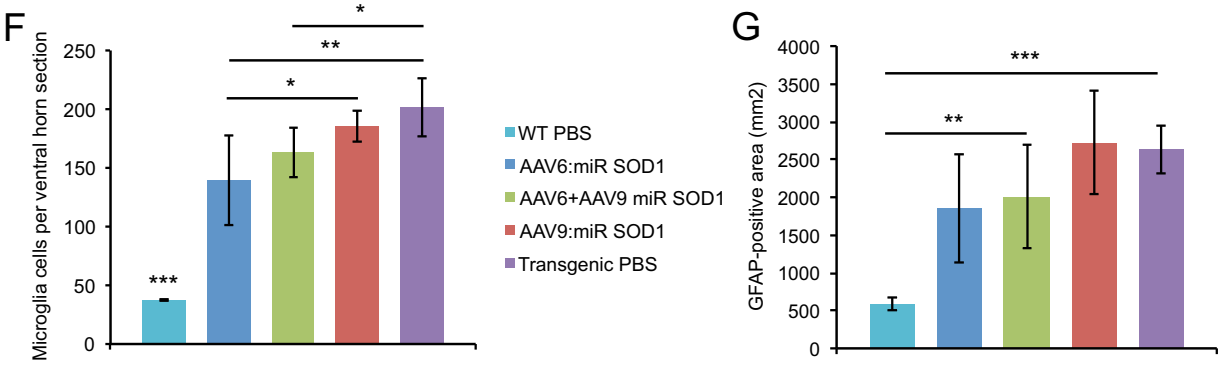

ChAT were captured to assess SOD1 silencing efficiency in motoneurons of AAV6:miR SOD1 mice. Mean human SOD1 fluorescence intensity measured within manually delimited ChAT- and RFP-positive motoneurons revealed significant reduction in human SOD1 expression in treated mice (Fig. 3B and D). Similarly, silencing was evaluated in GFAP-positive astrocytes coexpressing GFP following ICV delivery of AAV9-gfaABC$_1$D:GFP:miR SOD1. Here again, a significant decrease in human SOD1 fluorescence was found (Fig. 3C and E). These results suggest that miR SOD1 efficiently reduces human SOD1 levels in transduced cells of end-stage AAV-treated animals.

AAV-miR SOD1 protects motoneurons and rescues NMJ occupancy

Spinal cord sections were obtained from treated animals at end stage. Sections were stained with cresyl violet, which revealed many intact motoneurons despite the presence of cellular infiltrates suggestive of an ongoing inflammatory process (Fig. 4A). ChAT-positive motoneurons were counted in the cervical, thoracic, lumbar, and sacral regions of the spinal cord. As compared to WT and PBS-injected ^{G93A}SOD1 mice, we found remarkable preservation of motoneuron integrity at all levels of the spinal cord in AAV6:miR SOD1 (83–92% of WT values) and AAV6 + AAV9:miR SOD1 (73–88% of WT values) groups (Fig. 4B). In AAV9-gfaABC$_1$D:GFP:miR SOD1-injected animals, the number of motoneurons was lower than in AAV6-injected mice at all levels of the spinal cord (54–62% of WT values), although it remained significantly increased compared to PBS-injected ^{G93A}SOD1 mice (33–38% of WT values). NMJ integrity in gastrocnemius muscles was evaluated by measuring the percentage of bungarotoxin-positive motor end plates that colocalized with SV-2-positive motoneuron terminals. Remarkably, NMJs were rescued to >90% occupancy for all treated groups as compared to $12 \pm 4\%$ for control ^{G93A}SOD1 mice (Fig. 4C). These data are consistent with the rescue of CMAP values and swimming performance of miR SOD1-treated animals. Inflammation was present in control and treated ^{G93A}SOD1 mice at end stage, as revealed by Iba1 and GFAP immunostainings of microglial and astroglial cells (Fig. 4D and E). Interestingly, however, the number of activated microglial cells in lumbar ventral horns was significantly reduced in AAV6:miR SOD1 and AAV6 + AAV9:miR SOD1 animals (Fig. 4F). To evaluate astroglial activation, GFAP-positive total area was measured in lumbar ventral horns. Similar to microglial activation, astrogliosis was decreased in the animals injected with AAV6:miR SOD1, although this trend did not reach statistical significance (Fig. 4G).

Muscle fiber diameter is significantly increased in AAV:miR SOD1-injected animals

Macroscopic view of triceps surae muscles of end-stage AAV6:miR SOD1 mice revealed increased muscle size with respect to PBS-injected ^{G93A}SOD1 mice (Fig. 5A). Hematoxylin and eosin staining of gastrocnemius muscle sections confirmed preserved muscle integrity (Fig. 5B–F). Patches of atrophied muscle fibers were, however, evident in the AAV9:miR SOD1 group (Fig. 5E). Measurement of individual muscle fiber area revealed a clear shift toward smaller fibers in PBS-injected ^{G93A}SOD1 mice (Fig. 5G). Remarkably, distribution of muscle fiber sizes for AAV6:miR SOD1 and AAV6 + AAV9:miR SOD1 groups largely matched that of WT mice. Although a pool of small size fibers was observed in AAV9:miR SOD1 animals, most of the muscle remained protected from atrophy (Fig. 5G). Overall, muscle fiber area of treated animals was significantly larger than control ^{G93A}SOD1 mice. It remained, however, statistically smaller than WT controls (Fig. 5H). As we found almost complete protection of NMJ occupancy, fiber size reduction could be attributable to maintained expression of mutant SOD1 in the muscle. Indeed, there was no significant reduction in human SOD1

Figure 4. Motoneuron counts and neuromuscular junction occupancy are significantly increased in all treated groups despite astrogliosis and microglial activation. (A) Cresyl violet staining of lumbar ventral horns showing motoneuron preservation despite inflammatory infiltration for all treated conditions. Scale bar: 100 μm. (B) Motoneuron counts per spinal cord section for vector-injected and control animals at cervical, thoracic, lumbar, and sacral levels. Motoneuron numbers are significantly increased at all levels in treated animals. AAV6:miR SOD1: $n = 9$, AAV6 + AAV9:miR SOD1: $n = 7$, AAV9:miR SOD1: $n = 8$, transgenic PBS: $n = 12$, WT PBS: $n = 14$. (C) Neuromuscular junction integrity expressed as percentage of SV-2-positive motoneuron terminals to bungarotoxin-positive motor end plates. Innervation is preserved in all vector-injected conditions ($n = 3$ per group). (D) Microglial activation evidenced by increased Iba1 immunostaining in transgenic animals. Scale bar: 100 μm. (E) GFAP immunostaining showing astroglial activation. (F) Microglial counts per lumbar ventral horn in vector-injected and control mice. Note that AAV6:miR SOD1 and AAV6 + AAV9:miR SOD1 conditions display significantly decreased microglial activation compared to transgenic PBS and AAV9:miR SOD1 groups; $n = 5$ animals per group, 10 ventral horns per animal. (G) Astrogliosis determined by measuring GFAP-positive total area in lumbar ventral horns of vector-injected and control animals; $n = 5$ animals per group, 10 ventral horns per animal. Data are expressed as mean $\pm$ standard deviation. $^*P < 0.05$, $^{**}P < 0.01$, $^{***}P < 0.001$, one-way ANOVA and Newman–Keuls post hoc test. SOD1, superoxide dismutase 1.

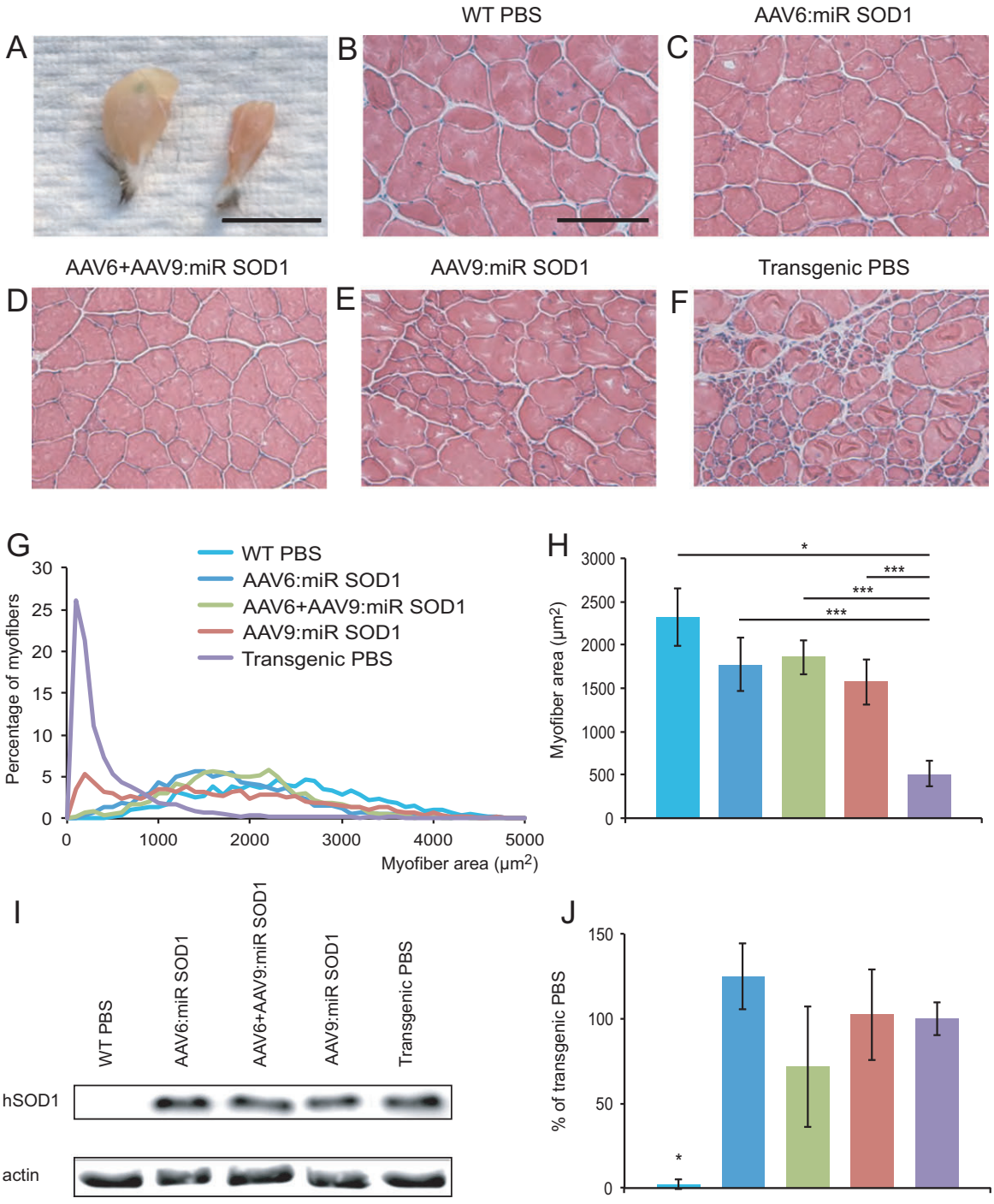

Figure 5. Muscle fiber diameter is significantly greater in vector-injected mice compared to control transgenic animals. (A) Macroscopic view of gastrocnemius muscles from an AAV6:miR SOD1- versus a PBS-injected ^{G93A}SOD1 mouse. Scale bar: 1 cm. (B–F) Muscle sections from treated and control animals reveal conserved muscle integrity in vector-injected animals. Scale bar: 100 μm. (G) Distribution of myofiber section area in the gastrocnemius muscle demonstrates protection from muscle atrophy. Small diameter fibers are only observed in transgenic control animals and, to a lesser extent, in AAV9:miR SOD1-injected animals. (H) Average muscle fiber area for vector- and PBS-injected groups. Area was measured for all individual fibers, in five 600 × 400 μm fields of view per animal; $n = 5$ animals per group. (I) Western blot representing human SOD1 levels in the quadriceps of mice injected ICV with AAV vectors compared to PBS-injected controls. (J) Quantification of human SOD1 levels expressed as percentage of human SOD1 amount detected in PBS-injected transgenic mice. Values are represented as mean ± standard deviation. *$P < 0.05$, ***$P < 0.001$, one-way ANOVA and Newman–Keuls post hoc test. SOD1, superoxide dismutase 1.

expression in the quadriceps muscle of mice injected with either AAV6 or AAV9:miR SOD1 vectors (Fig. 5I and J).

Intrathecal injection of AAV:miR SOD1 to adult ^{G93A}SOD1 mice shows protection of the neuromuscular function

To further evaluate the therapeutic relevance of our SOD1 silencing approach, we next assessed the benefits of administering miR SOD1 to adult ^{G93A}SOD1 mice. In order to achieve highest transduction levels in the spinal cord we performed IT lumbar injections of AAV9 viral vectors. Based on a preliminary study, we selected the AAV9 serotype because it showed the best transduction profile of the spinal cord following IT injection in adult mice. The cmv promoter was used for preferential expression of the miR SOD1 sequence in motoneurons, whereas the gfaABC$_1$D promoter was used for astrocyte-specific expression (Fig. 6A). ^{G93A}SOD1 mice were IT injected at the age of 5 weeks with 2.4E12 vg of AAV9-cmv:RFP:miR SOD1 or AAV9-gfaABC$_1$D:GFP:miR SOD1. We chose the time point at which the first pathological effects become detectable by electromyography.

Mice were then followed on a weekly basis to monitor neuromuscular functions. Globally, CMAP measurements in triceps surae muscles revealed improved muscle response in treated animals compared to PBS-injected ^{G93A}SOD1 mice (Fig. 6B). Overall, a significant difference was also observed between AAV9-cmv- and AAV9-gfaABC$_1$D-injected animals ($P < 0.05$). For both miR: SOD1 treated groups, CMAP values initially dropped and then stabilized at the age of 60 days until mice had to be sacrificed. Mice injected with the AAV9-cmv:RFP:miR SOD1 vector had, however, slightly better neuromuscular responses, when compared to AAV9-gfaABC$_1$D. Indeed, CMAP values of AAV9-cmv-injected animals stabilized at around 75% of their initial values and statistically differed from control ^{G93A}SOD1 mice at 5 weeks post-injection. In comparison, the AAV9-gfaABC$_1$D group stabilized at 55% of their initial values and became statistically different from the control group at 9 weeks post-injection. At that age, miR: SOD1 treatment also translated into significantly improved swimming performance compared to PBS-injected transgenic mice (Fig. 6C). However, at the age of 140 days, two of the seven mice injected with AAV9-cmv:RFP:miR SOD1 suddenly showed a drastic decline in swimming abilities, which globally impacted the average performance of the group. For this last time point, no difference was observed in swimming performance between treated and control ^{G93A}SOD1 mice, in part because some mice showed difficulties to orient themselves in the pool. In the Rotarod test, motor activity was still significantly improved at P140 for both miR SOD1-injected groups compared to control transgenic mice (Fig. 6D).

Overall, the treatment did not delay disease onset, nor slow down disease progression (data not shown) and survival was similar for treated and untreated ^{G93A}SOD1 mice (Fig. 6E).

At the histological level, AAV9-cmv:RFP:miR SOD1 injection led to a significant protection of motor unit integrity (Fig. 6F). Silencing SOD1 predominantly in neuronal cells significantly increased by 30% the number of ChAT-positive motoneurons in the ventral horn (25.6 ± 1.5), compared to PBS-injected ^{G93A}SOD1 mice. In contrast, AAV9-gfaABC$_1$D:GFP:miR SOD1 had no significant effect on the number of motoneurons per section (18.1 ± 2.1) compared to control ALS mice (15.2 ± 2.7). At comparable injected doses, we found that the AAV9-cmv:RFP:miR SOD1 vector was significantly more protective than AAV9-gfaABC$_1$D in the lumbar region ($P < 0.001$). In the cervical region, the protective effect of AAV9-cmv:RFP:miR SOD1 injections remained minimal when compared to control ^{G93A}SOD1 mice (27 ± 0.9 vs. 20.9 ± 1.7 motoneurons per section), whereas AAV9-gfaABC$_1$D:GFP:miR SOD1 (21.7 ± 1.9) had no effect.

AAV9-cmv-based miR SOD1 expression also significantly preserved NMJ integrity in gastrocnemius muscles with $69.9 \pm 2.8\%$ of bungarotoxin-positive motor end plates colocalizing with VAChT-positive motoneuron terminals at end stage, as compared to only $26.2 \pm 3\%$ for the PBS-injected control group (Fig. 6G). Remarkably, NMJs were also significantly protected in the AAV9-gfaABC$_1$D:GFP:miR SOD1 group ($49.4 \pm 5.6\%$ of occupancy). The effect was, however, less pronounced than with the AAV9-cmv vector, and mirrored the observed difference in CMAP amplitude. Overall, injection of AAV: miR SOD1 vectors in adult mice provides long-lasting neuroprotection at the level of injection.

Discussion

We show here complete rescue of neuromuscular function in ALS ^{G93A}SOD1 mice following neonatal ICV administration of AAV vectors designed to express an artificial microRNA against human SOD1 in either motoneurons or astrocytes. Restored neuromuscular function is demonstrated in all treated groups by full normalization of both CMAP amplitude in the triceps surae, and swimming performance. Effective neuroprotection is confirmed in end-stage animals by histological analysis assessing motoneuron counts, NMJ occupancy and muscle fiber area. For all these parameters, silencing of human SOD1 following vector injection in mouse neonates demonstrates clear therapeutic efficacy. Therapeutic relevance of SOD1 silencing is further

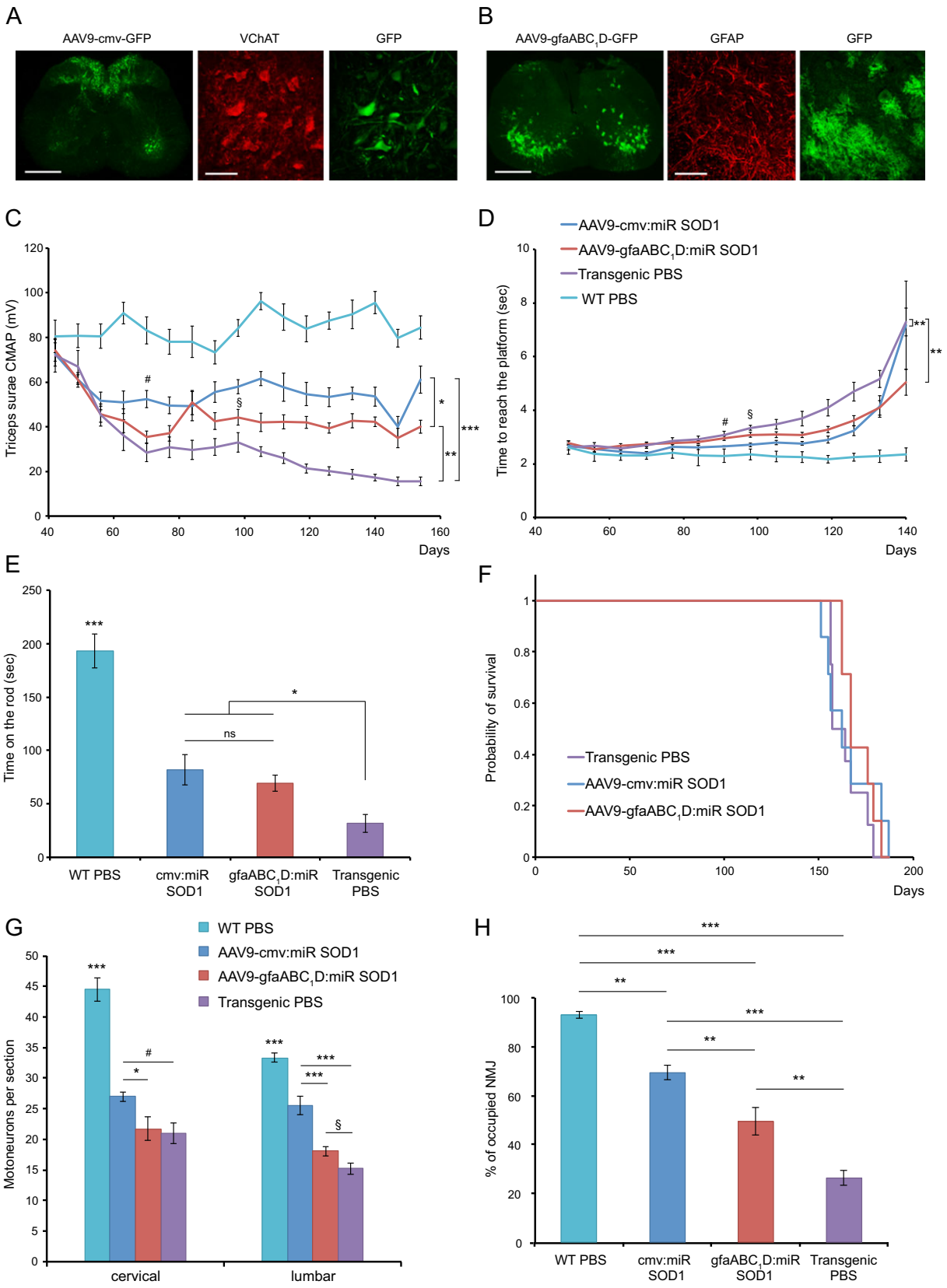

demonstrated following lumbar IT injection of miR SOD1 sequences to adult ^{G93A}SOD1 mice.

Moreover, our results indicate that selecting the cell type(s), to which silencing clues are targeted is important to obtain highest therapeutic efficacy. By injecting two different serotype/promoter combinations, we achieve different patterns of SOD1 silencing, predominantly targeting either motoneurons or astrocytes. Following injection of AAV vectors in both newborn and adult mice, motoneuron protection is highest when SOD1 is mainly silenced in motoneurons. Nevertheless, expression of miR SOD1 in astrocytes also leads to normalization of swimming performance and CMAP values, supporting a critical role for astroglial expression of mutated SOD1 in the decline of the neuromuscular function. Animals injected with AAV9-gfaABC$_1$D:GFP:miR SOD1 display an initial drop in CMAP amplitude that progressively recovers. ^{G93A}SOD1 ALS mice have a highly predictable course of denervation that takes place in two successive episodes. There is an initial pruning of fast-twitch fatigable (FF) motoneurons, resulting in the denervation of type IIb muscle fibers. Vacant NMJ are then partially reinnervated by the sprouting of fast-twitch fatigue-resistant (FR) and slow-twitch fatigue-resistant (S) motoneurons until FR motoneurons also start pruning their intramuscular nerve branches leading to a sustained loss of NMJ.[16,17] The initial decrease in CMAP amplitude observed in mice, where astrocytic SOD1 is suppressed likely reflects the pruning of FF motoneuron innervation, which would hence mainly depend on mechanisms intrinsic to motoneurons. Recovery of normal CMAP values indicates that SOD1 silencing in astrocytes might be protective against late denervation processes. Indeed, despite a lower degree of motoneuron and muscle fiber protection, NMJ occupancy is improved until end stage.

Remarkably, we observed very efficient neuroprotection when SOD1 is silenced in motoneurons, with 83–92% of motoneurons still present at end stage in neonatal ICV-injected animals. In comparison, astrocyte-specific SOD1 silencing protects motoneurons to a lower degree (54–62% of WT values), although motoneuron survival is still improved when compared to control ^{G93A}SOD1 mice (33–38% of WT values). A similar difference in neuroprotective effects between the two vectors was observed at the lumbar level following IT injection of adult mice. Motoneuron loss in AAV9:gfaABC$_1$D:miR SOD1 mice could be a consequence of early neuromuscular denervation and axonal dying-back of FF motoneurons, which is likely to be a cell autonomous process.

Although motoneuron loss is the culprit of ALS phenotype, astrogliosis, and microglial activation are major disease markers. Overexpression of miR SOD1 in motoneurons and/or astrocytes of newborn mice does not prevent neuroinflammation at end stage. However, microglial activation is hampered when miR SOD1 is expressed in motoneurons. Microglial cells become activated notably in response to motoneuron degeneration.[18] Hence, the extensive motoneuron protection observed in AAV6:miR SOD1 and AAV6 + AAV9:miR SOD1 groups might limit microglial activation. Surprisingly, downregu-

Figure 6. Intrathecal injection of AAV-miR SOD1 to adult ALS mice shows therapeutic benefits. (A and B) Represented are lumbar sections of mice injected intrathecally with AAV9 coding for GFP. The cmv promoter leads to transgene expression preferentially in VChAT-positive motoneurons (A), whereas the gfaABC$_1$D promoter specifically targets astrocytes (B). Scale bar: whole spinal cord, 500 μm; close-up, 80 μm. (C) CMAP values were recorded from triceps surae of treated and control animals. Neuromuscular function is partially rescued in miR: SOD1-injected animals when compared to transgenic controls. Overall, significant group effect is observed between all conditions. Note that CMAP values of the AAV9-cmv:miR SOD1 and AAV9-gfaABC$_1$D:miR SOD1 animals start to be statistically different from values obtained for the PBS-injected ^{G93A}SOD1 mice at weeks 5 (#) and 9 (§) postinjection, respectively. (D) Evaluation of weekly swimming performances reveals overall improved motor abilities of treated animals compared to transgenic PBS mice. Significant difference in the time necessary to reach platform is observed starting at 8 weeks postinjection for the AAV9-cmv:miR SOD1 group (#) and 9 weeks postinjection for the AAV9-gfaABC$_1$D:miR SOD1 group (§). No significant difference with the transgenic PBS mice is observed for the last time point. (E) At day 140, AAV-injected animals show significantly superior forced motor activity when using the Rotarod test as compared to transgenic PBS-injected mice. No significant difference is observed between the two miR SOD1-injected groups (F) Kaplan–Meier survival curve shows no difference in survival between treated and PBS-injected ALS mice. (G) Motoneuron counts per spinal cord section for AAV9-injected and control animals at cervical and lumbar levels. At the lumbar level motoneuron numbers are significantly increased for the AAV9-cmv:miR SOD1 group when compared to AAV9-gfaABC$_1$D:miR SOD1 and transgenic control animals. A trend toward improved motoneuron survival is observed for the AAV9-gfaABC$_1$D:miR SOD1 group at the lumbar level (§; $P = 0.05$). At the cervical level the AAV9-cmv:miR SOD1 group counts significantly more motoneurons than the AAV9-gfaABC$_1$D:miR SOD1 group but only a trend toward improved survival (#; $P = 0.06$) is observed when compared to control ALS mice. (H) Neuromuscular junction integrity expressed as percentage of VAChT-positive motoneuron terminals to bungarotoxin-positive motor end plates. Innervation is partially preserved in both AAV: miR SOD1-injected groups, with significant difference being observed between the AAV9-cmv and the AAV9-gfaABC$_1$D animals. (D–H) AAV9-cmv:miR SOD1: $n = 6$, AAV9-gfaABC$_1$D:miR SOD1: $n = 7$, transgenic PBS: $n = 8$, WT PBS: $n = 9$. Data are expressed as mean ± standard errors of the mean deviation. One-way ANOVA and Newman–Keuls post hoc test. Two-way ANOVA and Newman–Keuls post hoc test was used for evaluation of the significance of group effect on CMAP values and swimming performance. $^*P < 0.05$, $^{**}P < 0.01$, $^{***}P < 0.001$. SOD1, superoxide dismutase 1; CMAP, compound muscular action potentials; ALS, amyotrophic lateral sclerosis.

lation of SOD1 expression in astrocytes does not diminish astroglial activation. These results suggest that motoneuron dysfunction plays a preponderant role in inducing inflammation in ^{G93A}SOD1 mice. Overall our results support a critical role for astrocytes in ALS pathogenesis, albeit motoneurons remain a major target for AAV-based therapeutic interventions.

The impact on ^{G93A}SOD1 mice survival is an important parameter of treatment efficacy. Indeed, rescue of mutant SOD1-induced paralysis has remained a challenge since transgenic ^{G93A}SOD1 mice were developed almost 20 years ago.[4] For this proof-of-principle study we used the high-copy ^{G93A}SOD1 mice, bred on a pure C57BL/6 background, to promote the phenotypic uniformity within the groups. It is, however, difficult to compare groups in terms of lifespan as end stage criteria differ among control PBS and newborn-treated animals. Indeed, it appears that vector-injected mice do not die of hindlimb paralysis as typically observed in ^{G93A}SOD1 mice. Some animals instead displayed multiple systemic abnormalities including signs of ataxia, increased susceptibility to eye and skin infections as well as gastrointestinal complications. Preliminary analyses have not yet identified the origin of these dysfunctions. It is possible that other aspects of the ^{G93A}SOD1 phenotype have been revealed as treated mice survived the classical hindlimb paralysis observed in transgenic controls. On the other hand, these symptoms could be the consequence of treatment side effects.

By delivering recombinant AAVs in early postnatal days, we have maximized targeting of widespread distributed motoneurons and astrocytes. Moreover, early intervention is optimal to achieve therapeutic benefit in this proof-of-principle experiment. As determined by the peak of the weight curve, AAV-based motoneuronal SOD1 silencing significantly delays disease onset, whilst the depletion of SOD1 in astrocytes has no impact on early weight loss. The AAV9:miR SOD1 group, however, shows a prolonged early disease phase when compared to untreated ^{G93A}SOD1 mice. As AAV-treated animals do not appear to die of typical ALS symptoms, weight loss at terminal stage is most probably a consequence of pathogenic mechanisms distinct from muscle atrophy and paralysis-induced cachexia. Since mice of the AAV6:miR SOD1 group actually died before reaching 10% weight loss, it is not possible to determine if SOD1 silencing in MNs also has an impact on early disease phase. These results, however, support previous studies demonstrating that astrocytes play a key role in disease progression, whereas motoneurons are critical for initiation of disease processes.[9,15,19] Previous studies using Cre-mediated recombination to suppress SOD1 expression in motoneurons did not show a higher effect compared to targeting glial cells.[9,15] This discrepancy with respect to our results could be attributed to differences in the technology used to remove SOD1 expression. We have strong evidence that AAV-based RNAi against SOD1 can abolish SOD1 expression in a large proportion of spinal motoneurons. With the AAV9:gfaABC$_1$D:miR SOD1 vector, the percentage of astrocytes expressing the transgene is likely to be lower, which may limit therapeutic efficacy. In addition, we cannot exclude that AAV also silences SOD1 in other types of neurons, including upper motoneurons, and therefore further delays disease onset.

Silencing mutant SOD1 in motoneurons early in disease pathogenesis might target mechanisms upstream of glial cell activation and is sufficient to significantly improve disease outcome. However, determining the impact of cell-type-specific SOD1 silencing at later disease stages is crucial to design the most effective therapeutic strategy for human patients. Of importance, recent reports show promising results regarding silencing SOD1 at later disease stages, although the impact of silencing mutant proteins specifically in motoneurons versus astrocytes has not yet been addressed.[7,20] We here confirm the therapeutic relevance of our AAV-based SOD1 silencing approach following IT administration of miR SOD1 to adult ALS mice. Neuromuscular function is indeed significantly improved when compared to control transgenic mice. The results obtained on adult-injected mice support the observations made following ICV administration of therapeutic vectors to pups. With equal doses of vector, the AAV9-cmv-miR SOD1 vector, which preferentially targets motoneurons when administered to adult mice, reveals an overall increased therapeutic efficiency when compared to the astrocyte-specific AAV9-gfaABC$_1$D vector. This was most evident in terms of CMAP amplitude, end-stage motoneuron counts and in the preservation of the NMJ occupancy. These therapeutic benefits did, however, not translate into prolonged survival of treated ^{G93A}SOD1 mice. Most probably, IT lumbar injections of AAV-miR SOD1 did not allow targeting a sufficient amount of motoneurons or astrocytes along the spinal cord to significantly impact survival of high-copy ^{G93A}SOD1 C57BL/6 mice. Indeed, a neuroprotective effect following IT injection of AAV9-cmv-miR SOD1 was only observed locally in the lumbar region, close to the injection site. In the cervical spinal cord, motoneurons were less protected. It will be important to develop surgical procedures in larger animals to deliver the vector to enough motoneurons and/or astrocytes in order to reach the critical threshold for therapeutic efficacy. We injected AAV vectors to adult ^{G93A}SOD1 mice 2 weeks before the initial drop in CMAP value becomes significant and 5 weeks before the first significant decrease in swimming performance. It is encouraging that therapeutic benefits can be obtained when the treatment is applied close to or

after apparition of the first symptoms.[7, 20] Indeed, it is likely that the development of novel reliable biomarkers, such as microRNA profiles,[21] may allow future therapeutic approaches for ALS patients to be administered earlier in the disease process.

In conclusion, we show here full rescue of neuromuscular function in a severe ALS mouse model following neonatal ICV injection of AAV-miR SOD1. Moreover, direct comparison of AAV vectors for SOD1 silencing in motoneurons and astrocytes in newborn and adult animals reveals motoneurons as crucial therapeutic targets. These results establish the proof-of-principle for AAV-based therapeutic silencing approaches directed against mutated SOD1 and possibly other targets in ALS patients, emphasizing the potential of gene therapy against motoneuron diseases.

Acknowledgments

The authors thank Vivianne Padrun, Fabienne Pidoux, Christel Sadeghi, Philippe Colin, and Aline Aebi for technical assistance as well as Michael Brenner for kindly providing the gfaABC$_1$D promoter.

Author Contributions

E. D., J. A., and B. S. designed the experiments. E. D., J. A., and C. R. conducted the experiments. E. D., B. S., J. A., and C. R. analyzed the data. C. T. designed and cloned microRNA sequences in the pAAV backbones. E. D., B. S., J. A., and P. A. wrote the manuscript.

Conflict of Interest

None declared.

References

1. Rosen DR, Siddique T, Patterson D, et al. Mutations in Cu/Zn superoxide dismutase gene are associated with familial amyotrophic lateral sclerosis. Nature 1993;362:59–62.
2. Al-Chalabi A, Jones A, Troakes C, et al. The genetics and neuropathology of amyotrophic lateral sclerosis. Acta Neuropathol 2012;124:339–352.
3. Rothstein JD. Current hypotheses for the underlying biology of amyotrophic lateral sclerosis. Ann Neurol 2009;65(suppl 1):S3–S9.
4. Gurney ME, Pu H, Chiu AY, et al. Motor neuron degeneration in mice that express a human Cu,Zn superoxide dismutase mutation. Science 1994;264:1772–1775.
5. Raoul C, Abbas-Terki T, Bensadoun JC, et al. Lentiviral-mediated silencing of SOD1 through RNA interference retards disease onset and progression in a mouse model of ALS. Nat Med 2005;11:423–428.
6. Ralph GS, Radcliffe PA, Day DM, et al. Silencing mutant SOD1 using RNAi protects against neurodegeneration and extends survival in an ALS model. Nat Med 2005;11:429–433.
7. Foust KD, Salazar DL, Likhite S, et al. Therapeutic AAV9-mediated suppression of mutant SOD1 slows disease progression and extends survival in models of inherited ALS. Mol Ther 2013;21:2148–2159.
8. Lasiene J, Yamanaka K. Glial cells in amyotrophic lateral sclerosis. Neurol Res Int 2011;2011:718987.
9. Yamanaka K, Chun SJ, Boillee S, et al. Astrocytes as determinants of disease progression in inherited amyotrophic lateral sclerosis. Nat Neurosci 2008;11:251–253.
10. Wang L, Gutmann DH, Roos RP. Astrocyte loss of mutant SOD1 delays ALS disease onset and progression in G85R transgenic mice. Hum Mol Genet 2011;20:286–293.
11. Lepore AC, Rauck B, Dejea C, et al. Focal transplantation-based astrocyte replacement is neuroprotective in a model of motor neuron disease. Nat Neurosci 2008;11:1294–1301.
12. Boucherie C, Schafer S, Lavand'homme P, et al. Chimerization of astroglial population in the lumbar spinal cord after mesenchymal stem cell transplantation prolongs survival in a rat model of amyotrophic lateral sclerosis. J Neurosci Res 2009;87:2034–2046.
13. Dirren E, Towne CL, Setola V, et al. Intracerebroventricular injection of adeno-associated virus 6 and 9 vectors for cell type-specific transgene expression in the spinal cord. Hum Gene Ther 2014;25:109–120.
14. Scott S, Kranz JE, Cole J, et al. Design, power, and interpretation of studies in the standard murine model of ALS. Amyotroph Lateral Scler 2008;9:4–15.
15. Boillee S, Yamanaka K, Lobsiger CS, et al. Onset and progression in inherited ALS determined by motor neurons and microglia. Science 2006;312:1389–1392.
16. Pun S, Santos AF, Saxena S, et al. Selective vulnerability and pruning of phasic motoneuron axons in motoneuron disease alleviated by CNTF. Nat Neurosci 2006;9:408–419.
17. Kanning KC, Kaplan A, Henderson CE. Motor neuron diversity in development and disease. Annu Rev Neurosci 2010;33:409–440.
18. Henkel JS, Beers DR, Zhao W, Appel SH. Microglia in ALS: the good, the bad, and the resting. J Neuroimmune Pharmacol 2009;4:389–398.
19. Jaarsma D, Teuling E, Haasdijk ED, et al. Neuron-specific expression of mutant superoxide dismutase is sufficient to induce amyotrophic lateral sclerosis in transgenic mice. J Neurosci 2008;28:2075–2088.
20. Wang H, Yang B, Qiu L, et al. Widespread spinal cord transduction by intrathecal injection of rAAV delivers efficacious RNAi therapy for amyotrophic lateral sclerosis. Hum Mol Genet 2014;23:668–681.

21. Freischmidt A, Muller K, Zondler L, et al. Serum microRNAs in patients with genetic amyotrophic lateral sclerosis and pre-manifest mutation carriers. Brain 2014;137(Pt 11):2938–2950.

Supporting Information

Additional Supporting Information may be found in the online version of this article:

Figure S1. Behavioral, electrophysiological, and survival outcomes depend on the silencing efficiency of selected miR sequences. (A) Neuromuscular function as assessed by CMAP for control animals and animals overexpressing miR-b SOD1, a miR sequence with lesser silencing ability than miR SOD1. No significant difference is observed in CMAP evolution of mice overexpressing miR-b SOD1 in motoneurons and/or astrocytes as compared to PBS-injected transgenic littermates. A trend is, however, present as CMAP values of the AAV6:miR-b SOD1 group are consistently higher than transgenic controls. Indeed, AAV6:miR-b SOD1 mice are not significantly different from PBS-injected WT mice, in contrast to PBS-injected ^{G93A}SOD1 animals. (B) CMAP evolution over disease course in animals injected with a control scramble miR sequence. Note that there is no difference between vector- and PBS-injected transgenic animals. (C and D) Swimming ability of animals injected with miR-b SOD1 (C) or miR cont (D) compared to PBS-injected transgenic and WT animals. Significantly shorter swimming times are only achieved for the last time point in the AAV6:miR-b SOD1 and AAV6 + AAV9:miR-b SOD1 groups. (E and F) Kaplan–Meier survival curves for vector-injected versus PBS-injected mice of the miR-b (E) or miR cont group (F). Significant increase in survival is only achieved for AAV6 + AAV9:miR-b SOD1 mice (180 ± 9 days vs. 169 ± 9 days for PBS-injected ^{G93A}SOD1 mice). In comparison, AAV6:miR-b SOD1 mice lived up to 176 ± 7 days and AAV9:miR-b SOD1 mice up to 171 ± 11 days. AAV6:miR-b SOD1: $n = 11$, AAV9:miR-b SOD1: $n = 13$, AAV6 + AAV9:miR-b SOD1: $n = 12$, AAV6:miR cont: $n = 7$, AAV9:miR cont: $n = 9$, AAV6 + AAV9:miR cont: $n = 6$, transgenic PBS: $n = 14$, WT PBS: $n = 13$. Values are expressed as mean $\pm$ standard deviation. $^{***}P < 0.001$, repeated measure two-way ANOVA and Newman–Keuls post hoc test for CMAP, swimming performance and weight measurements. Nonparametric survival analysis was performed using Cox-Mantel test.

